2D/3D Simulation of macrosegregation: a comparison between codes on a small cavity and on a large ingot

Sylvain Gouttebroze, Weitao Liu, Michel Bellet, Hervé Combeau

Proc. MCWASP XI, 11th Int. Conf. on Modeling of Casting, Welding and Advanced Solidification Processes, Opio, France, May 28 - June 3, 2006, C.A. Gandin, M. Bellet (eds.), The Minerals, Metals & Materials Society, Warrendale, Pennsylvania, USA (2006) 227-234

2D/3D SIMULATION OF MACROSEGREGATION: A COMPARISON BETWEEN CODES ON A SMALL CAVITY AND ON A LARGE INGOT

Sylvain Gouttebroze[1], Weitao Liu[1], Michel Bellet[1], Hervé Combeau[2]

[1]Ecole des Mines de Paris, CEMEF, UMR CNRS 7635, F06904 Sophia Antipolis, France
[2]Ecole des Mines de Nancy, LSG2M, Parc de Saurupt, F54042 Nancy, France

Keywords: macrosegregation, solidification, finite elements, finite volume

Abstract

This paper presents the coupled resolution of momentum, energy and solute conservation equations, for binary alloys by three different codes. The microsegregation is governed by the lever rule and the liquid flow in the mushy zone is modeled by a Darcy law. A 2D FV code, SOLID, a 2D FE code, R2SOL and a 3D FE code, THERCAST, are compared on an academic case on which experimental measurements have been done by Hebditch and Hunt, and on a benchmark steel ingot for industrial application. An adaptive anisotropic remeshing technique is used in each FE codes. For both codes, this technique is shortly described.

Introduction

Conservation equations over the two-phase mushy domain involved in alloy solidification may be obtained either by the classical mixture theory [1, 2] or by spatial averaging techniques [3, 4]. While the former gives rise to simpler single-phase-like equations, the latter clarifies the relationship between macro and microscopic scale phenomena. But both theories lead to similar results. The main objective of the present work is the prediction of the macrosegregation pattern in solidifying binary alloys in ingots. To achieve this goal, a remeshing technique has been introduced in FE codes (R2SOL and THERCAST). After presenting the equations and the resolution strategy, we will describe the criteria used to define the mesh size and anisotropic factors. The results obtained by these two FE codes on two tests (small and large ingot) will be compared to those of SOLID, a finite volume two-dimensional code developed by Combeau *et al* [5]. The codes have been previously compared on the same small ingot but without remeshing [6]. We will see here the improvements particularly on segregated channels prediction. Adaptive remeshing is also a necessary step to simulate large ingot solidification with F.E.M. So our new efficient remeshing strategy opens the way to introduce the coupling with solid deformation and air gap formation.

Governing Equations and Resolution

The analysis of fluid flow, temperature and solute distribution in a solidifying material amounts to the coupled solution of the equations stating the conservation of mass, momentum, energy and solute. The following numerical discretization and scheme concern only the two FE codes R2SOL and THERCAST. For information on SOLID numerical resolution we refer to [5].

Simplifying Hypotheses. The present model of binary-alloy solidification is based upon the following hypotheses. We refer to [7] for a discussion on their range of validity.

- The liquid flow is laminar, Newtonian, with a constant-viscosity μ. The solid phase is fixed and non deformable.
- The mushy region is modeled as an isotropic porous medium saturated with liquid (*i.e.*: $g_s + g_l = 1$, g_s denoting the volumic solid fraction and g_l the liquid one). Its permeability K is defined by the Carman-Kozeny formula, in which λ_2 is the secondary dendrite arm spacing: $\mathrm{K} = \lambda_2^{\,2} g_l^{\,3} (1-g_l)^{-2} / 180$.
- The solid and liquid phase densities are equal ($\rho=\rho_s=\rho_l$) and constant ($\rho=\rho_0$), except in the buoyancy term of the momentum equation where density depends on the temperature T and the solute concentration in liquid w_l according to the Boussinesq approximation $\rho = \rho_0(1-\beta_T(T-T_0)-\beta_w(w_l-w_{l0}))$, in which β_T and β_w are the thermal and solutal expansion coefficients, respectively.
- The microsegregation is governed by the lever rule. Given k the partition coefficient at solid-liquid interface, the average solute concentration w is related to w_l by:

$$w = g_l w_l + g_s k w_l = (g_l + (1-g_l)k) w_l \tag{1}$$

- The phase diagram is linearized, the liquidus slope m being constant and T_m being the melting temperature of the pure substance, we have:

$$T = T_m + m w_l \tag{2}$$

Mass Conservation. Denoting $\boldsymbol{V}$ the average velocity (here equal to the average liquid velocity, since the solid is fixed), the mass conservation equation is reduced to:

$$\nabla \cdot \mathbf{V} = 0 \tag{3}$$

Momentum Conservation. The classical mixture theory [1, 2] yields (4), while the averaging technique [3, 4] leads to (5)

$$\rho_0 \frac{\partial \mathbf{V}}{\partial t} + \rho_0 \nabla \cdot (\mathbf{V} \times \mathbf{V}) = \nabla \cdot (\mu \nabla \mathbf{V}) - \nabla p + \rho \mathbf{g} - \frac{\mu}{\mathrm{K}} \mathbf{V} \tag{4}$$

$$\rho_0 \frac{\partial \mathbf{V}}{\partial t} + \frac{\rho_0}{g_l} \nabla \cdot (\mathbf{V} \times \mathbf{V}) = \nabla \cdot (\mu \nabla \mathbf{V}) - g_l \nabla p + g_l \rho \mathbf{g} - \frac{\mu}{\mathrm{K}} g_l \mathbf{V} \tag{5}$$

where p is pressure and $\boldsymbol{g}$ the gravity vector. While the FV code SOLID and R2SOL are based on (5), THERCAST is originally based on (4), but also considers (5). The time-discretized form of (4) and (5) is obtained using the Euler-backward scheme. The spatial discretization is carried out using a P1/P1 tetrahedral finite element, with SUPG-PSPG stabilization [8].

Solute Conservation. Redistribution of solute is governed by equation (6), where ε is a diffusion coefficient, usually negligible (and kept arbitrarily small). Following Voller *et al* [7], the time-integrated version of (6) is written as (7).

$$\frac{\partial w}{\partial t} + \boldsymbol{V}.\nabla w_l - \nabla.(\varepsilon \nabla w_l) = 0 \tag{6}$$

$$\frac{w^t - w^{t-\Delta t}}{\Delta t} + \nabla w.\boldsymbol{V} + \nabla.(\varepsilon \nabla w) = \nabla\left(w^* - w_l^*\right)\boldsymbol{V} - \nabla.\left[\varepsilon \nabla\left(w^* - w_l^*\right)\right] \tag{7}$$

It will be seen further that the super-index * refers either to the value at the previous time instant $t-\Delta t$, in case of weak coupling, or to the latest iterative estimate in case of strong coupling. The weak form of (7) is solved by the Streamline Upwind/Petrov-Galerkin method.

Energy Conservation. The heat equation can be written as follows, given the above assumptions:

$$\rho\left(\frac{\partial H}{\partial t}+\nabla H_l.\boldsymbol{V}\right)-\nabla.(\lambda\nabla T)=0 \tag{8}$$

where λ is the average thermal conductivity and H is the average enthalpy:

$$H=\int_{T_0}^{T} c_p d\tau + g_l L \tag{9}$$

c_p being the specific heat (assumed constant) and L the latent heat. Linear tetrahedral elements and an Euler-backward scheme are used to discretize (8) in space and time, respectively. In each element, a constant value of $\partial H / \partial T$ is used, in order to solve a weak form of (8) for the nodal enthalpies, also using SUPG.

Resolution Strategy. In the context of a Eulerian (fixed mesh) resolution, the resolution algorithm over a time increment is described in box 1. It can be seen that some resolution steps are iteratively chained in case of full coupling. The superscription * indicates the current estimate during iterations. In case of weak coupling the step 1 is solved with w assumed constant and equal to the local value given by (7) just before the point begins to solidify.

1)	Resolution of energy conservation (weak form of (8))	$\rightarrow H^*$
2)	Resolution of solute average conservation (weak form of (7))	$\rightarrow w^*$
3)	Local resolution, at each node, of microsegregation ((1), (2) and (9))	$\rightarrow g_l^*,\ T^*,\ w_l^*$
4)	Resolution of momentum conservation (weak form of (4) or (5))	$\rightarrow \boldsymbol{V}^*,\ p^*$
5)	If full coupling, iterate steps 1) to 4) until convergence. At the end, assign:	$var^{t+\Delta t} \leftarrow var^*$

Box 1. Summary of the main procedures carried out during a time increment.

Adaptive Anisotropic Remeshing Strategy

The goal is a dynamic mesh refinement in the mushy zone in order to provide an accurate prediction of the flow field. With these conditions, the prediction of macrosegregation could be done efficiently. The main idea of the adaptive remeshing is to identify during the simulation the areas that need a remeshing, depending on some determinant variables. Here the strategy is mainly based on the mushy zone, where the transport of solute is essential, and on the dynamic boundary layer zone in front of the solidification front. So the first step of this strategy is to identify these areas and to calculate the needed mesh size.

The objective local mesh size h is determined by three criteria for mushy and liquid areas:

- Gradient of liquid fraction $\|\nabla g_l\|$
- Gradient of mean concentration $\|\nabla w\|$
- Gradient of the velocity norm $\|\nabla\|\mathbf{V}\|\|$

For each parameter, two threshold values and two corresponding mesh sizes are defined, and linear interpolation is made between these points:

$$h=\begin{cases} h_2 & \text{if } V_{cr} > S_2 \\ \dfrac{S_2-V_{cr}}{S_2-S_1}\cdot(h_1-h_2)+h_2 & \text{if } S_2 \geq V_{cr} \geq S_1 \\ h_1 & \text{if } V_{cr} < S_1 \end{cases}$$

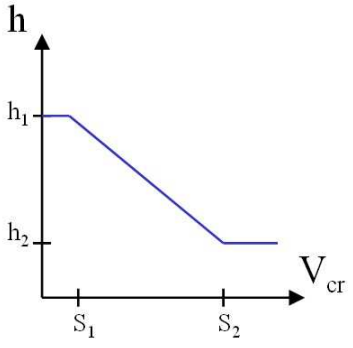

Figure 1. Evolution of the mesh with the selected criterion value

The mesh size in solid area is calculated by a maximum change in mean concentration in the element. Then the objective mesh size is the minimum of the three values obtained using the three different criteria. Using this strategy we obtain an objective mesh size at each node that combines the information coming from resolution of energy, solute and momentum equations.
In the second step the anisotropy factors are calculated. The local anisotropy factors are the orientation of the mesh and the elongation factor. The first one controls the direction in which the objective mesh size is applied and the second one determines the objective mesh size in the two other directions. The domain is divided in three different areas:

- the solid zone, controled by the mean concentration gradient;
- the mushy zone, controled by the liquid fraction gradient;
- the liquid zone, controled by the velocity.

So, in each zone, the mesh orientation is given by a selected vector (e.g. liquid fraction gradient in the mushy zone). Then the elongation factor is calculated using the direction change of these vectors in the element. The smaller the angle is (e.g. unidirectional flow), the larger the elongation of the element is. Finally the objective metric is smoothed to regularize the mesh sizes before generating a new mesh. This adaptive anisotropic remeshing allows us to refine the mesh in critical areas and is also easy to implement and to adjust to particular cases. Its efficiency has been proved for a simple benchmark case and for a medium ingot case (see ref. [11]). The above description corresponds to THERCAST strategy but R2SOL remeshing module follows the same lines.

Applications

Hebditch and Hunt Test. The first case consists of the solidification of Pb-48wt%Sn and Sn-5wt%Pb ingots studied by Hebditch and Hunt [9]. In this test, the alloy is solidified in a parallelepipedic cavity (6 cm high, 10 cm long and 1.3 cm thick, see fig. 2), which is insulated on all surfaces except the thinnest lateral one. This test has already served as a benchmark to evaluate the results of 2D and 3D solidification codes [4, 6]. Here it is studied with the 2D codes R2SOL and SOLID, and with the 3D code THERCAST, but using a pseudo-2D (one layer of 3D elements). In this case, we assume that the fluid flow in the largest midplane section is not influenced by the two parallel walls of the cavity. This hypothesis will be demonstrated by the full 3D simulation with THERCAST. The physical data used in the calculation can be found in the literature [4].

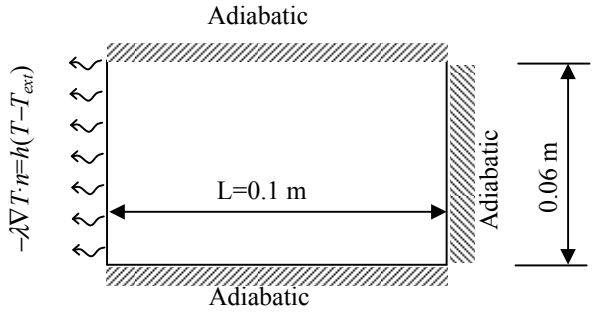

Figure 2. Hebditch and Hunt test problem.

Sn-5wt%Pb Alloy. The computation is performed applying the adaptive remeshing strategy for the R2SOL simulation and a structured fixed mesh for SOLID and THERCAST simulation. The mesh used in THERCAST is 3D with a symmetry plane to simulate just the half of the cavity. The mesh is refined near the back wall and in the channel on the bottom. A constant time step of 0.05 s is used, which is the same as in SOLID. The differences between the codes are shown in fig. 3. The prediction of the channel is effective in each simulation but the application of the remeshing strategy with R2SOL increases the extent of the segregated

channels, compared with THERCAST (for more details see [10]). Assuming a sticking condition at the wall, fig. 3-d) demonstrates that the segregation is really 2D with the formation of segregated bands in the whole width of the cavity. The boundary layer at the wall has a negligible effect on the segregation. So, in this case, a 2D simulation is a good approximation.

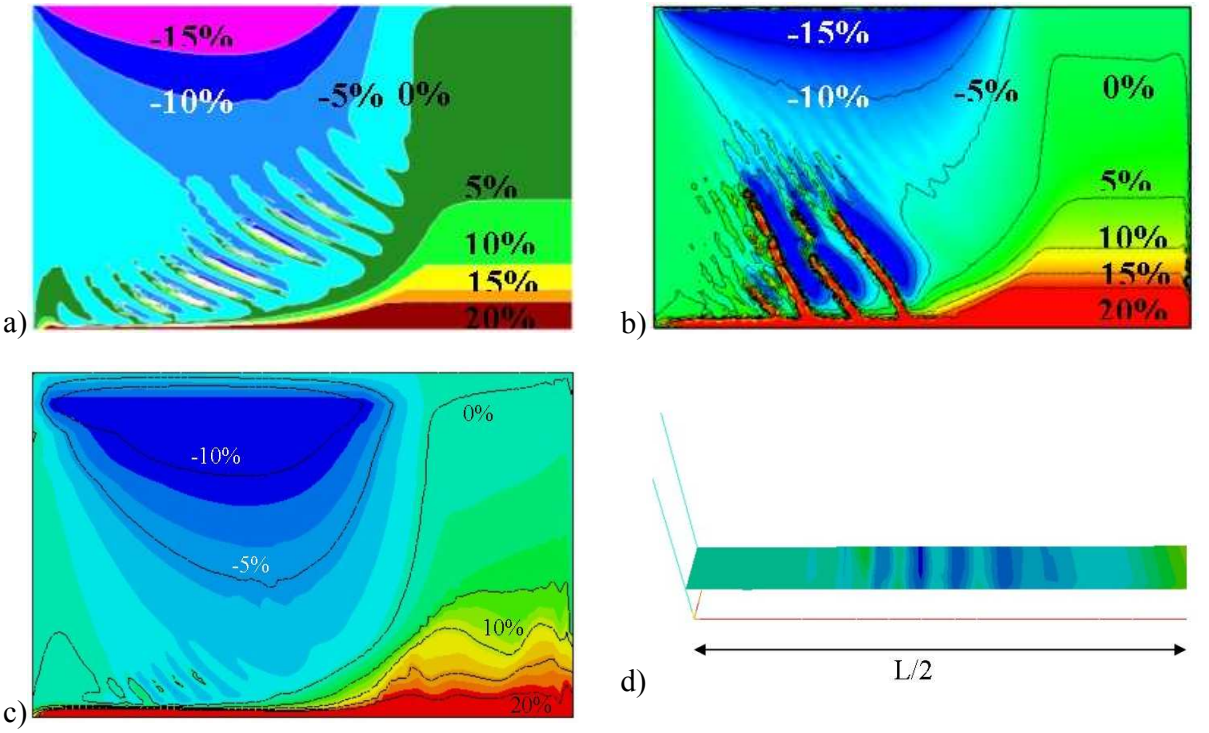

Figure 3. Relative variation of Pb average concentration at 400s: a) with SOLID, b) with R2SOL, c) with THERCAST, d) THERCAST results on a section at z=5mm.

Pb-48wt%Sn Alloy. The calculation is run with an adaptive finite element mesh for R2SOL and THERCAST and with a structured mesh for SOLID. Moreover, the mesh used in THERCAST simulation is a pseudo-2D mesh, which means that there is only one element in the width of the cavity and that the front and back faces are symmetry planes. The time step is 0.1 s. The segregation patterns at 400 s are plotted in fig. 4 (end of solidification at 1200s). The three simulations results are close, a small difference appearing in THERCAST simulation at the top right where the segregation is lower and the isolines more distorted. The gap is even clearer on the profiles in the section z = 55 mm (5 mm from top) on fig 4-f. But in the other sections, simulations are in good agreement (fig 4-d and e). Due to a different treatment of the boundary conditions for the solute equation between FE and FV, we can see a border effect on the right hand side of the R2SOL profile. This point was also presented by Ahmad *et al.* [4].
Despite this discrepancy in the top section in Pb-48%Sn alloy ingot, these two academic cases allow us to validate the implementation of macrosegregation and of adaptive remeshing. As illustrated, the advantages of the remeshing strategy are a more precise solution, a more stable code and a better capture of high gradients areas (particularly segregated channels).

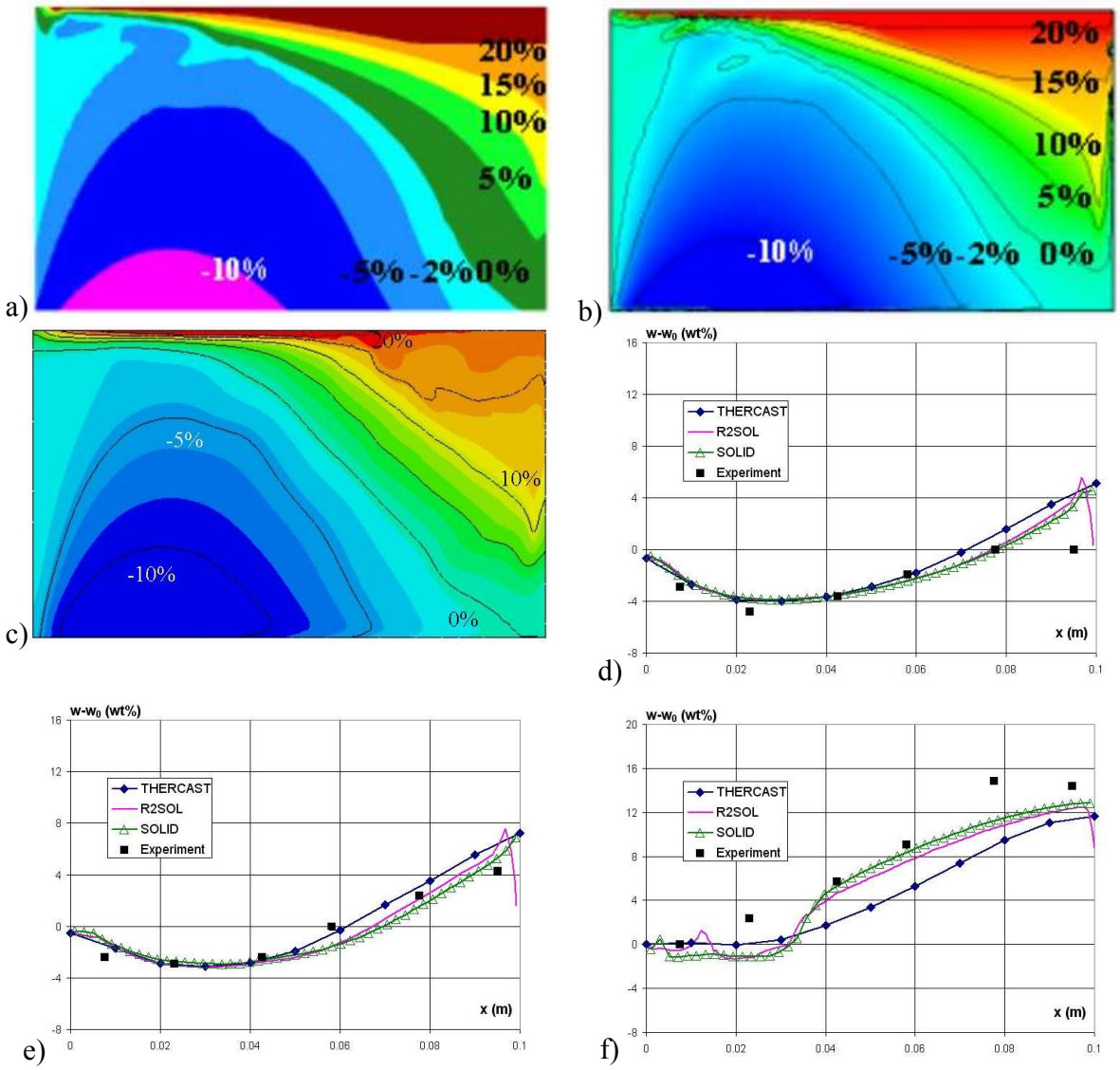

Figure 4. Relative variation of Sn average concentration at 400s: a) with SOLID, b) with R2SOL, c) with THERCAST, comparison with experimental measurements on a section at z=25mm (d), z=35mm (e) and z=55mm (f) at the end of solidification.

Benchmark Steel Ingot. For the last application, we consider the solidification of a binary carbon steel alloy in a cylindrical ingot, which is a simplified version of an octogonal 3.3 tons ingots produced by Aubert et Duval. Material properties, geometry and boundary conditions are presented on fig. 5. The ingot top surface is adiabatic. The adaptive remeshing strategy is applied using a minimum mesh size of 1 mm in the mushy zone and a maximum mesh size equal to 30 mm in the solid zone. For this case the comparison is made only between R2SOL and SOLID because of the huge calculation time needed for a sufficiently fine mesh in 3D.
The numerical gap between a small cavity and a large ingot is really important for FE codes. Actually it seems necessary to maintain a small element size in the mushy zone so a huge mesh must be used without adaptive remeshing. On the contrary the finite volume seems to react differently and a classical mesh, with a smaller number of nodes, is sufficient (this conclusion was also drawn from test on H-H cavity). But the predictions of macrosegregation present some discrepancies as shown on fig. 6. A positive segregation appears in the bottom in R2SOL simulation and also at the level of the refractory part. The axial segregation has the same shape but with higher maximum and minimum values in R2SOL simulation.

To conclude this comparison, it is currently difficult to discriminate the results and decide which code gives the best results. A deeper study of the ingot solidification, of the flow field evolution and formation of macrosegregation along time is certainly necessary to identify the key points of these differences. But the use of adaptive remeshing in R2SOL makes us able to simulate efficiently the macrosegregation and so to obtain crucial information on this process.

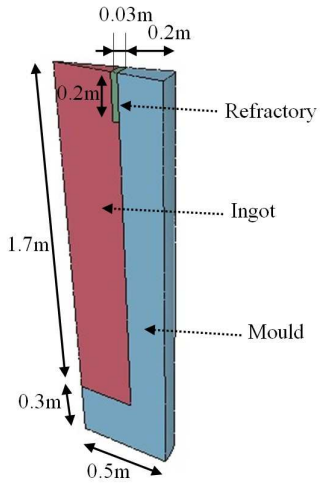

Thermal data		Mold	Refr
Thermal conductivity, λ	$W.m^{-1}.K^{-1}$	30	0
Specific heat, c_p	$J.kg^{-1}.K^{-1}$	540	10
Volumetric mass, ρ_0	$Kg.m^{-3}$	7000	13
Calculation parameters			
Initial temperature	°C	250	2
Heat transfer coefficient, h Between mold/air, refractory/air	$W.m^{-2}.K^{-1}$	100	1
External temperature, T_{ext}	°C	50	5

Phase diagram data		
Nominal mass fraction, w_0	wt.pct	0.38
Melting temperature, T_f	°C	1538
Eutectic temperature, T_{eut}	°C	1338
Liquidus slope, m	°C.wt.pct^{-1}	-80
Partition coefficient, k		0.18
Eutectic mass fraction, w_{eut}	wt.pct	2.5
Thermal data		
Thermal conductivity, λ	$W.m^{-1}.K^{-1}$	35
Specific heat, c_p	$J.kg^{-1}.K^{-1}$	715
Latent heat, L	$J.kg^{-1}$	0.309×1
Other characteristics		
Reference volumetric mass, ρ_0	$Kg.m^{-3}$	7060
Reference temperature, T_{ref}	°C	1522
Thermal expansion coefficient, β_T	K^{-1}	-8.85×1
Solutal expansion coefficient, β_w	wt.pct^{-1}	-4.1643×1
Dynamic viscosity, μ	Pa.s	0.42×10
Secondary dendrite arm spacing, λ_2	m	1.0×10
Calculation parameters		
Initial temperature	°C	1525
Time step	s	0.1
Heat transfer coefficient, h between ingot/mold, ingot/refractory	$W.m^{-2}.K^{-1}$	500
Gravity, **g**	$m.s^{-2}$	9.81
Diffusion coefficient in liquid, D_l	$m^2.s^{-1}$	1×10^{-9}

Figure 5. Materials properties and boundary conditions for the benchmark ingot simulation.

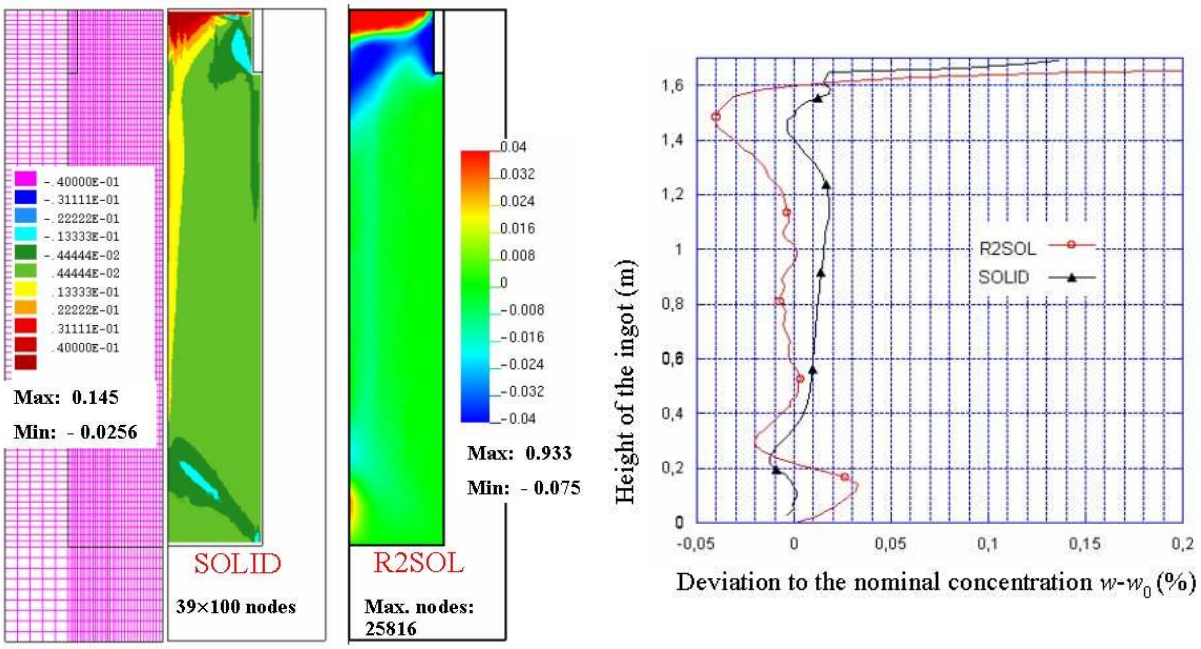

Figure 6. Macrosegregation pattern and axial segregation at the end of the solidification.

Conclusion

After a first implementation of the macrosegregation in the two codes R2SOL and THERCAST, another step has been made by the introduction of a remeshing strategy. The improvement in the results was demonstrated in small cavity and also in a large ingot. But the solidification in large ingot needs more investigation to understand the flow complexity and its coupling with the macrosegregation. Future work will be dedicated to deeper investigations regarding remeshing influence, to the extension to multiconstituent alloys and to the application to industrial castings for sensibility studies.

Acknowledgement

This work has been supported by the French Ministry of Industry, the French Technical Center of Casting Industries (CTIF) and the companies Arcelor-Irsid, Ascometal, Fonderie Atlantique Industrie, Aubert & Duval Alliages, Erasteel, Industeel and PSA.

References

1. C. Prakash and V. Voller, On the Numerical Solution of Continuum Mixture Equations Describing Binary Solid-Liquid Phase Change, *Num. Heat Transfer B* 15 (1989) 171-189.

2. W.D. Bennon and F.P. Incropera, A Continuum Model for Momentum, Heat and Species Transport in Binary Solid-Liquid Phase Change Systems – I. Model Formulation, *Int. J. Heat Mass Transfer* 30 (1987) 2161-2170.

3. J. Ni and C. Beckermann, A Volume-Averaged Two-Phase Model for Transport Phenomena during Solidification, *Metall. Trans.* 22B (1991) 349-361.

4. N. Ahmad, H. Combeau, J.-L. Desbiolles, T. Jalanti, G. Lesoult, M. Rappaz and C. Stomp, Numerical Simulation of Macrosegregation: a Comparison between Finite Volume Method and Finite Element Method Predictions and a Confrontation with Experiments, *Metall. and Mat. Trans.* 29A (1997) 617-630.

5. H. Combeau, F. Roch, J. C. Chevrier, I. Poitrault and G. Lesoult, Numerical Study of Heat and Mass ransfer during Solidification of Steel Ingots, In: *Advanced Computational Methods in Heat Transfer*, ed. L. C. Wrobel, Springer-Verlag, New York (1990) 79-90.

6. M. Bellet, V.D. Fachinotti, S. Gouttebroze, W. Liu, H. Combeau, A 3D-FEM model solving thermomechanics and macrosegregation in binary alloys solidification, Proc. Symposium on Solidification Processes and Microstructures, in Honor of Wilfried Kurz, TMS Annual Meeting, Charlotte (NC, USA) march 2004, M. Rappaz, C. Beckermann & R. Trivedi (eds.), The Minerals, Metals & Materials Society, pp. 41-46, 2004.

7. V.R. Voller, A.D. Brent, C. Prakash, The Modelling of Heat, Mass and Solute Transport in Solidification Systems, *Int. J. Heat Mass Transfer* 32 (1989) 1719-1731.

8. T.E. Tezduyar, and Y. Osawa, Finite element stabilization parameters computed from element matrices and vectors, Comput. Methods Appl. Mech. Engrg. 190 (2000), pp. 411-430

9. D.J. Hebditch, J.D. Hunt, Observations of ingot macrosegregation on model systems. *Metall. Trans*. 5 (1974) 1557-1564.

10. W. Liu, Finite element modelling of macrosegregation and thermomechnanical phenonmena in solidification processes. Ph.D. thesis, Ecole des Mines de Paris, 2005.

11. S. Gouttebroze, Modélisation 3D par éléments finis de la macroségrégation lors de la solidification d'alliages binaries. Ph.D. thesis, Ecole des Mines de Paris, 2005.